Research Article | Vol. 28, No. 9 / 27 April 2020 / Optics Express 13721
Optics EXPRESS

Passively synchronized mode-locked fiber lasers for coherent anti-Stokes Raman imaging

KANGWEN YANG,[1] YUE SHEN,[1] JIANPENG AO,[2] SHIKAI ZHENG,[1] QIANG HAO,[1] KUN HUANG,[1] MINBIAO JI,[2] AND HEPING ZENG[1,3,4,5,*]

[1]*Shanghai Key Laboratory of Modern Optical System, and Engineering Research Center of Optical Instrument and System, Ministry of Education, School of Optical Electrical and Computer Engineering, University of Shanghai for Science and Technology, Shanghai 200093, China*
[2]*State Key Laboratory of Surface Physics and Department of Physics, Human Phenome Institute, Multiscale Research Institute of Complex Systems, Academy for Engineering and Technology, Key Laboratory of Micro and Nano Photonic Structures (Ministry of Education), Fudan University, Shanghai 200433, China*
[3]*Chongqing Institute of East China Normal University, Chongqing 401121, China*
[4]*State Key Laboratory of Precision Spectroscopy, East China Normal University, Shanghai 200062, China*
[5]*Jinan Institute of Quantum Technology, Jinan 250000, China*
[*]*hpzeng@phy.ecnu.edu.cn*

Abstract: We have proposed and implemented a polarization-maintaining passively synchronized fiber laser system, which could deliver tunable dual-color picosecond pulses by including a frequency-doubling module and a spectral broadening module. Specifically, the output from the involved Er-doped fiber laser were used to generate second-harmonic pulses at 790 nm with a quadratic nonlinear crystal. In parallel, the amplified pulses from the synchronized Yb-doped fiber laser were launched into a 150-m single mode fiber, which resulted in not only substantial spectral bandwidth broadening from 0.1 to 20.1 nm, but also a significant Raman-induced signal around 1080 nm. Consequently, narrow spectra from 1018-1051 nm and 1070-1095 nm could be continuously tuned via a tunable bandpass filter, corresponding to Raman bonds from 2835-3143 cm^{-1} and 3312-3525 cm^{-1}. Finally, the achieved tunable synchronized pulses enabled us to microscopically examine mouse ear samples based on coherent anti-Stokes Raman and second harmonic generation imaging. Therefore, our tunable passively-synchronized fiber laser system would be promising to provide a simple and compact laser source for subsequent coherent Raman microscopy.

1. Introduction

Coherent anti-Stokes Raman scattering spectroscopy (CARS) is a powerful tool in detecting chemical bonds with high sensitivity and fast speed than spontaneous Raman imaging modalities [1–4], thus being widely used in various research fields such as brain tumor analysis [5], disease pathology [6], and 2D material imaging [7]. Among existing methods for acquiring the CARS signal, single band CARS utilizing synchronized dual-color picosecond pulses is still the most common and straightforward way [8]. In this scheme, the frequency difference between excitation lasers is continuously tuned, then the corresponding CARS signal at each Raman bond is detected and finally Raman spectrum can be probed. The key parameters of dual-color laser for CARS imaging are narrow spectral bandwidth and large wavelength tuning range for resolving Raman bonds with high spectral resolution and wide detection range. These requirement can be satisfied by widely-used synchronized solid-state lasers or bulky optical parametric oscillators. However, their large size, complex free-space optical arrangement and high environmental sensitivity have limited many CARS applications in well-maintained optical lab [8].

#389728 https://doi.org/10.1364/OE.389728
Journal © 2020 Received 10 Feb 2020; revised 14 Apr 2020; accepted 14 Apr 2020; published 22 Apr 2020

Optics EXPRESS

Recent development of compact laser system provides wavelength-tunable, dual-color laser pulses by means of photonic crystal fiber (PCF) based nonlinear frequency conversion methods, thus accelerating the wide application of this technique in optical lab and clinical environment [8–13]. For example, supercontinuum generation (SC) is a widely adopt technique, which typically requires femtosecond pulse and highly nonlinear fiber. The generated broadband spectrum is post-filtered to obtain new wavelengths. Although the tuning range is very broad, the average power at each wavelength is limited due to low spectral density. Soliton self-frequency shift in anomalous dispersion fiber can convert the wavelength of input femtosecond pulse to longer region with a high efficiency. However, the temporal duration of soliton is very short, thus generation of narrow band spectrum with high average power is rather difficult. Recently developed fiber optical parametric oscillator or amplifier has been reported to achieve wide tunability [14,15], flexible repetition rate [16] or even watt-level average power [17]. However, the spectral bandwidth is inevitably broadened with the increased pump power due to competition of complex nonlinear effects and the conversion efficiency is limited.

Alternatively, using dual-color picosecond pulses from two independent lasers by either active or passive synchronization scheme to excite the sample's vibrational band is a more straightforward method. For active scheme, subfemtosecond timing jitter between two mode-locked Ti:sapphire lasers has been reported by utilizing fast-bandwidth servo loop [18]. This technology enables tight pulse synchronization of two solid-state lasers or fiber lasers, its usefulness has been verified for CARS microscopy [19,20]. However, precise delay detection and fast phase-locking of active synchronization increase the system complexity. As for passive scheme, the nonlinear effect inside the fiber provides a fast response mechanism, thus establishes a more compact system. In inchoate demonstrations, passive synchronized fiber lasers were not polarization maintained (PM) and the cavity tolerance range was very short, making it very sensitive to environmental disturbance [21,22]. To solve this, our group has demonstrated passive synchronization for PM fiber lasers and significantly enlarged the cavity tolerance range [23,24].

In this paper, we established a passive synchronization system between picosecond Er- and Yb-doped fiber lasers. A nonlinear crystal was used to obtain second harmonic generation (SHG) of Er-doped fiber laser at 790 nm as the pump laser for CARS. As for the Stokes laser, an active spectral broadening (ASB) module and an optical bandpass (BPF) filter were added after Yb-doped fiber laser to achieve narrow spectral bandwidth and large tuning range for resolving Raman bands with high resolution and wide range. As a result, tunable Yb-doped laser pulses from 1018-1051 nm and 1070-1095 nm with spectral bandwidth of 0.3 nm were obtained. Using this laser source, CARS and SHG imaging of mouse ear sample were demonstrated.

2. Experimental setup

The experimental setup of passive-synchronized fiber lasers used for CARS imaging is shown in Fig. 1. It was comprised of Er- and Yb-doped fiber oscillators (EDFO/YDFO), fiber amplifiers and a SHG module, an ASB module and an optical BPF, and finally a laser scanning microscopy. Both PM fiber oscillators had figure-9 arrangements and could be passively mode-locked by nonlinear amplifying loop mirror. The gain fiber for EDFO was 1.5-m erbium doped fiber from Liekki (Er 80-4/125-HD-PM) with a peak core absorption of 80 dB/m at 1530 nm. The fiber lengths of circular part and linear part for EDFO were 11.8 m and 2.4 m, respectively. As for the YDFO, the gain fiber was 1.5-m ytterbium doped fiber from Nufern (PM-YSF-HI-HP) with a peak core absorption of 250 dB/m at 975 nm. The fiber lengths of circular part and linear part were 12.4 m and 2.1 m, respectively. The tuning range of collimators inside the cavity was 2 cm without affecting the mode-locking state. The detailed information can be found in our previous work [25,26]. The fiber Bragg grating (FBG) used for Er- and Yb-doped oscillator had a central wavelength of 1579.5 and 1029.5 nm, respectively. Two single mode PM fiber amplifiers were added after EDFO for power scaling. The gain fiber lengths for both Er- and Yb-doped

Optics EXPRESS

amplifier were 1.5 m. A small portion (5%) of the output pulses from amplified Er-doped laser were separated by a fiber coupler for passive synchronization. The other part (95%) of the output pulses were focused onto a periodically-poled lithium niobate (PPLN) crystal for SHG.

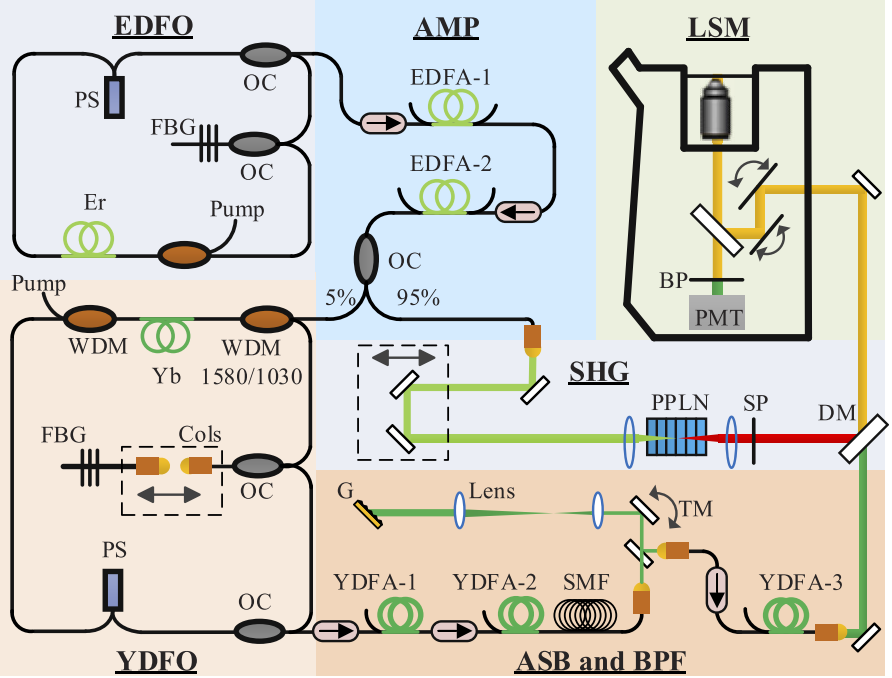

Fig. 1. Experimental setup. EDFO: Er-doped fiber oscillator; YDFO: Yb-doped fiber oscillator; AMP: amplifiers; SHG: second harmonic generation; ASB: active spectral broadening module; BPF: bandpass filter; SP: short pass filter; LSM: laser scanning microscopy; PS: phase shifter; OC: optical coupler; G: grating; SMF: single mode fiber; WDM: wavelength division multiplexer; TM: tunable mirror; PMT: photomultiplier tube.

Passive synchronization of two mode-locked lasers are realized in a master-slave configuration. The master laser pulses from Er-doped fiber amplifiers are injected into the Yb-doped slave laser cavity by a wavelength division multiplexer. The YDFO had the similar structure as the EDFO except for a pair of fiber collimators inside the cavity. By precisely changing the distance between fiber collimators to match the master cavity length, passive synchronization of two mode-locked fiber lasers could be achieved. The related mechanism relies on the cross-phase modulation in the gain fiber, which acts as a fast intensity modulator and force the YDFO to oscillate synchronously with the EDFO.

The synchronized pulses from YDFO were then sent into a home-built ASB module, which consisted of two fiber amplifiers and 150-m single mode PM fiber. After that, an optical BPF consisting of a tunable mirror, two achromatic lenses and a refractive grating with grating period of 1200 lines/mm was used to select certain spectral part from broadened spectrum. The optical pulses were reflected by the tunable mirror to the 4*f* relay lenses, which imaged the mirror plane on the reflection grating in the Littrow configuration. The grating diffracted optical pulses with slight vertical misalignment. Then these optical pulses went through the lenses and reflected again by the tunable mirror. We used another mirror and a fiber collimator to reflect and collect the output beam. Changing the angle of the tunable mirror would cause the change of incident angle on the grating, thus wavelength tuning can be achieved [27]. Another Yb-doped fiber amplifier was built to compensate power loss of this filter. Then the frequency doubled laser

Optics EXPRESS

pulses from Er branch and wavelength tunable laser pulses from Yb branch were combined by a dichroic mirror as pump and Stokes laser respectively, and sent to a commercial microscope for nonlinear biomedical imaging.

3. Experimental results

3.1. Output characteristics of Er and Yb oscillators

Figure 2 shows the spectral and temporal characteristics of laser pulses from EDFO, YDFO and corresponding fiber amplifiers. Both fiber lasers had the same repetition rate of 12.4 MHz. The spectrum of the EDFO was centered at 1579.5 nm with a full width at half maximum (FWHM) of 0.14 nm, corresponding to a Fourier transform limited pulse width of 25.6 ps. After two-stage amplifier, the average power was increased from 0.8 to 228 mW and the spectrum was broadened to 1.7 nm due to self-phase modulation (SPM), as shown with the shaped area in Fig. 2(a). The pulse duration after amplification was measured to be 26.0 ps by an autocorrelator, as shown in Fig. 2(c), which is slightly broadened due to the accumulated fiber dispersion. The YDFO had a spectral bandwidth of 0.10 nm centered at 1029.5 nm. The corresponding Fourier transform limited pulse width was 16.0 ps. The cascaded two-stage amplifier boosted the average power from 1.0 to 268 mW with a broadened spectral bandwidth of 0.70 nm, as shown in Fig. 2(b). The temporal duration of amplified pulse was 22.3 ps due to accumulated normal dispersion, as shown in Fig. 2(d).

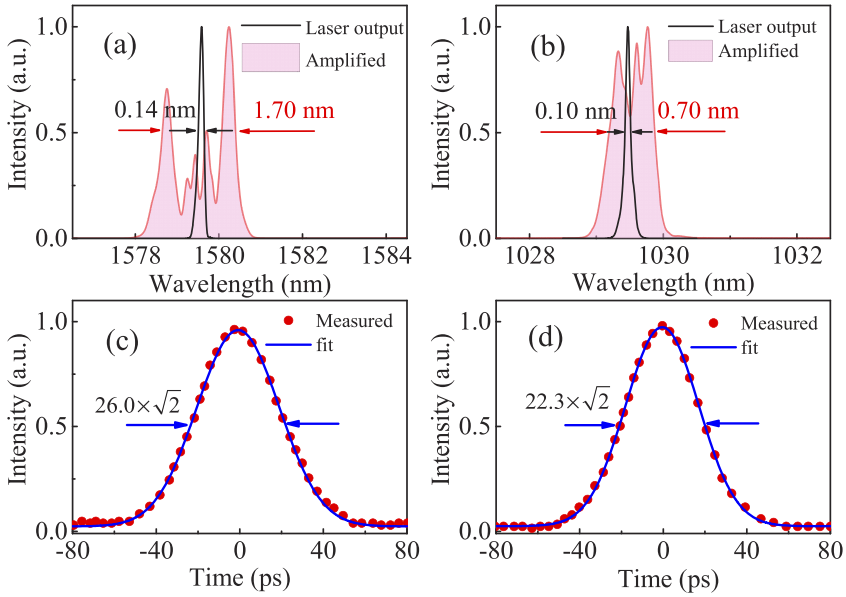

Fig. 2. Output spectra of Er-doped (a) and Yb-doped (b) laser pulses from oscillator (black line) and after amplifier (red shaped area). Autocorrelation trace for Er-doped (c) and Yb-doped (d) laser pulses.

It is noteworthy that the central wavelengths of two fiber lasers were determined by inter-cavity FBGs to match the vibrational energy level of CH_3. Meanwhile, the bandwidths of FBGs were chosen to be 0.2 nm to generate picosecond pulses with narrow spectral bandwidth. The relative longer temporal pulse width would be easier to handle for fiber amplification and delivery due to the reduced nonlinearity and accumulated dispersion, while the corresponding narrow spectral bandwidth would be preferable to obtain high spectral resolution for CARS. Moreover, the

Optics EXPRESS

cavity mismatch range for two passively synchronized picosecond lasers is longer than that for two femtosecond oscillators, thus long-term stable synchronization of two picosecond lasers is achieved.

3.2. Second harmonic generation of Er laser

Next we turn to analyze the SHG performance for Er-doped fiber laser. After fiber amplifiers, SHG experiment was conducted to obtain laser pulses at 790 nm. The 200-mW laser pulses were firstly coupled to free space by a fiber collimator and then focused on a PPLN crystal by an achromatic aspheric lens with a focal length of 30 mm. The grating period and the length of the PPLN was 20.22 μm and 10 mm, respectively. Another achromatic aspheric lens (focal length: 30 mm) and an optical short pass filter (cutoff wavelength: 1000 nm) were used to collimate and select the SHG laser pulses. The output power and corresponding conversion efficiency were shown in Fig. 3(a). The maximum average power was 41.8 mW with a conversion efficiency of 21%. Figure 3(b) shows the autocorrelation trace of frequency-doubled pulse, the temporal duration is 16.2 ps if we consider Gaussian fitting. The corresponding spectrum is shown in the insert, revealing a central wavelength of 789.8 nm and a spectral bandwidth of 0.88 nm.

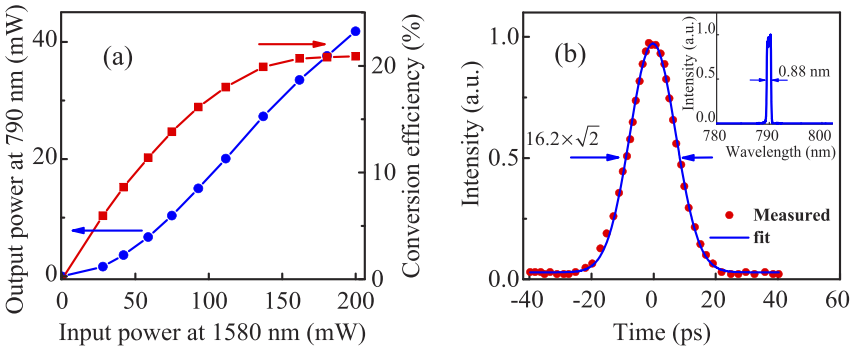

Fig. 3. (a) Output power and corresponding conversion efficiency for second harmonic generation. (b) Autocorrelation trace and spectrum of second harmonic laser pulses.

3.3. Performance of active spectral broadening module

In the following, we will investigate the performance of our active spectral broadening module. Figures 4(a)-(e) show the 10-dB spectral broadening evolution as the increase of the average power after two-stage Yb-doped fiber amplifier measured by an optical spectrum analyzer (OSA 201C, Thorlabs). Depending on the output powers and the corresponding nonlinear effects, the spectral evolution process can be roughly divided into three steps: SPM dominated spectral broadening, four-wave mixing (FWM) dominated spectral smoothing and stimulated Raman scattering (SRS) dominated new spectral component emergence [28]. In the beginning, the output spectrum of the laser pulses went through an almost symmetrical broadening from 0.3 to 6.5 nm with the increase of the output power from 1.0 to 70 mW. In this case, SPM and cross-phase modulation play the dominant roles for spectral evolution, thus exhibiting a multi-peak spectral shape with high intensity on the edge and low intensity in the middle [29,30]. With further increase of output power from 70 to 140 mW, the spectrum continued to broaden and became smooth due to FWM and intra-pulse Raman scattering. The combination of multiple nonlinear effects contribute to the generation of flattened spectrum in this process [31,32]. Once the output power exceeded to 210 mW, the spectral band located in longer wavelength range started to emerge due to SRS effect. Further increase of output power to 280 mW would strength SRS process, exhibiting a wide spectral component from 1070-1095 nm [33].

Optics EXPRESS

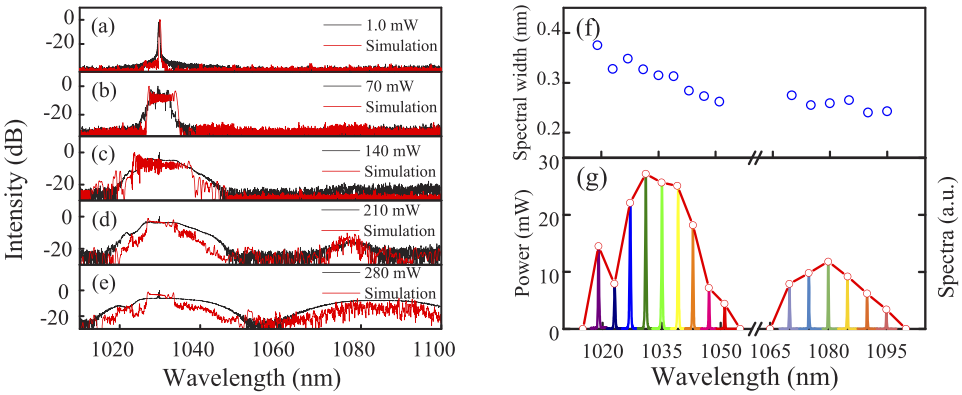

Fig. 4. (a)-(e) Measured (black lines) and simulated (red lines) spectral broadening evolution of laser pulses at various average powers from 1.0 to 280 mW. (f) Spectral widths and (g) powers of amplified laser pulse at different wavelengths.

For better understanding this spectral broadening process, we conducted theoretical simulation by using commercially available software Fiberdesk. The simulation model included an input pump pulse and 150-m single mode fiber. For different output powers, we changed the input pump energies correspondingly. The temporal duration of the input pump pulse was set to 22.3 ps. The mode field diameter and propagation loss was set to 6.6 μm and 0.0018/m, respectively. Nonlinear effects such as dispersion, Raman, SPM, self-steepening were activated during the simulation. The nonlinear refractive index coefficient n_2 was set to 2.3×10^{-20} m^2/W, which is the typical value for silica fiber. All the parameters were the same as those in the experiment. As the red curves shown in Figs. 4(a)-(e), the simulation results agree well with the experimental measurements.

In order to achieve wavelength tunability, the spectrally broadened laser pulses were coupled into an optical BPF. The basic configuration and operation principle have been discussed in previous publications [34]. By tuning the reflective angle of the tunable mirror, the incident angle on the diffraction grating can be changed, resulting a continuous tuning of the central wavelength. The spectral bandwidth of the filter can be optimized by changing the beam diameter and grating density. In our experiment, the spectral bandwidths of filtered laser pulses were around 0.3 nm, as shown in Fig. 4(f). Due to the insertion and filtering loss, another fiber amplifier was added to compensate the average power. The output power can be amplified to larger than 20 mW at wavelength range of 1026-1042 nm. The pulse width was measured to be 6.5 ps. Further amplification would give rise to spectral broadening at these wavelengths. As for the wavelengths of 1070-1095 nm, the amplified output power was around 6 mW, further increase of the pump power would introduce unwanted amplified spontaneous emission around 1036 nm. By adding spectral filter in fiber amplifier, this noise could be suppressed thus higher output power would be possible.

3.4. Coherent anti-Stokes Raman and second harmonic generation imaging

Once passive synchronization is achieved, both lasers can operate stably for days. Then we used these synchronized fiber lasers for single-band CARS and SHG imaging of unstained fresh mouse ear skin sample. For convenience, we denote the 790-nm laser pulses as the pump while the 1030-nm laser pulses are called Stokes. A free-space optical delay line was inserted in the Stokes branch to ensure temporal overlapping of pulses from two synchronized fiber lasers. Meanwhile, a dichroic mirror (790/1030 nm) was used to combine the pump and Stokes laser spatially. After that, dual-color laser pulses were injected to a commercial microscope (Olympus, FV1200)

Optics EXPRESS

for nonlinear imaging. The image acquisition rate was 2 µs/pixel according to the single-point integration time. The image size was 512×512. Due to the redundant time in the experiment, the time required to obtain an image was 1.08 s. In our manuscript, no averaging had been applied to any of the images. The numerical aperture of micro objective was 1.2, corresponding to an image resolution of about 400 nm for the microscope. The spectral resolution for CARS image is about 17 cm^{-1}. The average power for the input pump and Stokes laser was set to 40 and 20 mW, respectively. Due to the transmission loss of mirrors inside the microscope, the average power for pump and Stokes laser on the sample was approximately 20 and 10 mW, respectively. In our experiment, we used epi-detection scheme for biomedical imaging. The objective used to focus dual-color laser pulses onto the sample had an amplification factor of 25 and a numerical aperture of 1.2. A short pass filter (700 nm) and a bandpass filter (640 ± 20 nm) were used to eliminate the background light.

Figures 5(a)-(c) show CARS imaging of skin surface cells from mouse ear. These cells are rich in lipids, ceramides, and cholesterol, which can cause strong CARS signal. The blue channel in Fig. 5(a) was acquired at the CH_3 stretching vibration of proteins (2930 cm^{-1}) while the green channel in Fig. 5(b) was at the CH_2 stretching vibration of lipids (2850 cm^{-1}). We can see that proteins are mainly distributed in the middle of the cell and lipids are mainly distributed at the edge, as shown in a combined image in Fig. 5(c). Then we changed the focal length to visualize the structures at different depths of the sample. As shown in Fig. 5(d), we can see that the sebaceous glands are composed of multiple cells and they surround a hair shaft. Our laser sources can excite not only CARS imaging by dual-color pulses, but also SHG imaging by Yb-doped laser pulse. After replacing the optical filter, we can observe the SHG signal under the same field of view in Fig. 5(e). The SHG signal is mainly generated by collagen in subcutaneous tissue. By combining CARS and SHG modalities, multimodal nonlinear imaging of the sample can be achieved, as shown in Fig. 5(f).

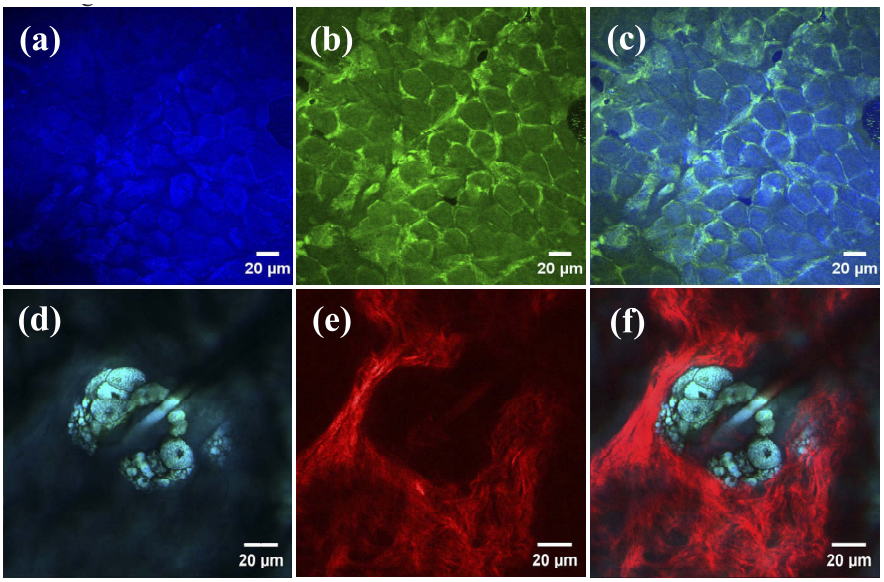

Fig. 5. CARS imaging of fresh mouse ear tissue at (a) 2930 cm^{-1}, (b) 2850 cm^{-1}. (c) Combined imaging of (a) and (b). (d) CARS and (e) SHG imaging of fresh mouse ear tissue. (f) Combined imaging of (d) and (e).

Optics EXPRESS

4. Discussions and conclusion

Our proposed passive synchronized fiber lasers have several advantages in practical usage. First, all the fibers used in this laser source are PM fibers, which exhibited better resistance to environmental mechanical vibration and temperature change. Therefore, stable mode-locking and amplification can be ensured. Second, the dual-color laser pulses were synchronized based on XPM effect in gain fiber, which has very fast response time thus timing jitter as low as 50 fs was achieved [23]. When the circulating pulse at 1030-nm encountered the injected pulse at 1580 nm, the optical collision between two pulses will result in an instantaneous phase shift by XPM effect. This phase shift would induce the frequency shift of the 1030-nm pulse and thus change the timing delay between the two pulses due to the group velocity dispersion of the fiber. This passive synchronization arrangement avoids precise detection of repetition difference and complex phase locking electronics in active method, which would simplify the control system of synchronized fiber laser source largely. What's more, the cavity mismatch tolerance between two fiber lasers is currently 1 mm, which is one or two orders larger than the cavity length shift of 10 hours in laboratory environment. By using shared cavity arrangement, the cavity mismatch tolerance can be increased to 16.2 mm, ensuring very long-term stable operation for passive synchronization [24].

Although PCF is the most widely used material for spectral broadening, especially in some supercontinuum generation experiment [35], we found SMF is more suitable for our scheme based on the following reasons. First, SMF can provide the same nonlinear effects used for spectral broadening with low splicing loss and easy operation. For spectral broadening of picosecond pulses in normal group velocity dispersion region, SPM, FWM and Raman scattering are the dominant mechanisms [36]. These effects can be utilized either in SMF or well-designed PCF. However, splicing between different fibers, especially hollow core or large mode area PCF is still a technical challenge, let alone the time-consuming design of fiber parameters and delicate fabrication of special fiber structure [29,37]. Second, although the nonlinear effects in SMF is weaker than those in PCF, we can strength these effects by increasing the fiber length. For example, 18.8-W, 21-ps input pulses were coupled into a 5-m PCF, resulting in a broadened spectral width of 100 nm. Lower input power of 1.49 W in the same case only generated a broadened spectrum of 5 nm [38]. As a contrast, we have used 0.28-W, 22.3-ps input pulses and successfully generated 20-nm broadened spectrum by 150-m SMF. The longer length of SMF compensated the lower input power and weaker nonlinear effects in our case.

The wavelength tuning modules are implemented outside the cavity, thus ensuring stable operation of both mode-locking and synchronization of laser oscillators when tuning the wavelength. Moreover, the tuning speed can be improved to kilohertz level by replacing the tunable mirror with a resonant galvanometer scanner, which would benefit fast biomedical imaging [27]. Currently, the achieved tuning range in our experiment just covered the CH vibration bonds in high Raman region. However, our proposed method can be used to access other Raman bonds by adding advanced spectral broadening module. For example, high nonlinear fiber or dispersion compensated fiber could be used to extend the wavelength range of Er-doped laser pulse before SHG. This would give the ability of not only tuning the Yb-doped laser, but also the Er-doped laser [12]. As a result, the available detection range of this dual-color synchronized laser source would be enlarged.

In conclusion, we reported an all-polarization-maintaining, passively synchronized dual-color fiber laser source for nonlinear biomedical imaging. Stable synchronization was achieved by injecting parts of Er-doped laser pulses into the Yb-doped laser cavity based on XPM mechanism. The Er-doped laser pulses were amplified and frequency-doubled to provide 790-nm pulses, while the Yb-doped laser pulses were amplified and spectrally broadened by 150-m SMF to provide seed pulses with wide spectrum. With cascade optical BPF and amplifier, the wavelength of Yb-doped fiber laser can be continuously tuned from 1018-1051 nm and 1070-1095 nm, covering the CH

Optics EXPRESS

vibration bonds (2835-3143 cm^{-1} and 3312-3525 cm^{-1}). Using our proposed laser source, CARS and SHG imaging of fresh mouse ear have been obtained, showing the capability of this laser on nonlinear biomedical imaging. With all-PM fiber design, stable passive synchronization and wavelength tunability, our proposed fiber laser system would be a compact and environmentally stable option for coherent Raman microscopy.

Funding

National Natural Science Foundation of China (11974248, 81671725, 61975033, 11727812); Program for Professor of Special Appointment (Eastern Scholar) at Shanghai Institutions of Higher Learning, Science and Technology Innovation Program of Basic Science Foundation of Shanghai (18JC1412000); Science and Technology Commission of Shanghai Municipality Major Project (2018SHZDZX01, 2017SHZDZX01); ZJLab.

Acknowledgement

The authors thank Prof. Yasuyuki Ozeki for generous help and insightful discussions.

Disclosures

The authors declare no conflicts of interest.

References

1. C. L. Evans and X. S. Xie, "Coherent anti-stokes Raman scattering microscopy: chemical imaging for biology and medicine," Annu. Rev. Anal. Chem. **1**(1), 883–909 (2008).
2. C. H. Camp Jr and M. T. Cicerone, "Chemically sensitive bioimaging with coherent Raman scattering," Nat. Photonics **9**(5), 295–305 (2015).
3. R. He, Y. Xu, L. Zhang, S. Ma, X. Wang, D. Ye, and M. Ji, "Dual-phase stimulated Raman scattering microscopy for real-time two-color imaging," Optica **4**(1), 44–47 (2017).
4. Y. Yang, L. Chen, and M. Ji, "Stimulated Raman scattering microscopy for rapid brain tumor histology," J. Innov. Opt. Heal. Sci. **10**(05), 1730010 (2017).
5. T. Meyer, N. Bergner, C. Bielecki, C. Krafft, D. Akimov, B. F. Romeike, R. Reichart, R. Kalff, B. Dietzek, and J. Popp, "Nonlinear microscopy, infrared, and Raman microspectroscopy for brain tumor analysis," J. Biomed. Opt. **16**(2), 021113 (2011).
6. M. Ji, M. Arbel, L. Zhang, C. W. Freudiger, S. S. Hou, D. Lin, X. Yang, B. J. Bacskai, and X. S. Xie, "Label-free imaging of amyloid plaques in Alzheimer's disease with stimulated Raman scattering microscopy," Sci. Adv. **4**(11), eaat7715 (2018).
7. J. Ling, X. Miao, Y. Sun, Y. Feng, L. Zhang, Z. Sun, and M. Ji, "Vibrational Imaging and Quantification of Two-Dimensional Hexagonal Boron Nitride with Stimulated Raman Scattering," ACS Nano **13**(12), 14033–14040 (2019).
8. T. Gottschall, T. Meyer, M. Baumgartl, C. Jauregui, M. Schmitt, J. Popp, J. Limpert, and A. Tünnermann, "Fiber-based light sources for biomedical applications of coherent anti-Stokes Raman scattering microscopy," Laser Photonics Rev. **9**(5), 435–451 (2015).
9. H. Tu, Y. Liu, D. Turchinovich, M. Marjanovic, J. K. Lyngsø, J. Lægsgaard, E. J. Chaney, Y. Zhao, S. You, W. L. Wilson, B. Xu, M. Dantus, and S. A. Boppart, "Stain-free histopathology by programmable supercontinuum pulses," Nat. Photonics **10**(8), 534–540 (2016).
10. K. Yang, S. Zheng, Y. Wu, P. Ye, K. Huang, Q. Hao, and H. Zeng, "Low-repetition-rate all-fiber integrated optical parametric oscillator for coherent anti-Stokes Raman spectroscopy," Opt. Express **26**(13), 17519–17528 (2018).
11. X. Chen, S. Yang, S. Ding, M. Chen, and H. Chen, "Instantaneous dynamics of a fiber optical parametric oscillator within its initiating process," IEEE Photonics Technol. Lett. **31**(13), 1088–1091 (2019).
12. C. W. Freudiger, W. Yang, G. R. Holtom, N. Peyghambarian, X. S. Xie, and K. Q. Kieu, "Stimulated Raman scattering microscopy with a robust fibre laser source," Nat. Photonics **8**(2), 153–159 (2014).
13. M. Andreana, T. Le, A. K. Hansen, A. J. Verhoef, O. B. Jensen, P. E. Andersen, P. Slezak, W. Drexler, A. Fernández, and A. Unterhuber, "Epi-detecting label-free multimodal imaging platform using a compact diode-pumped femtosecond solid-state laser," J. Biomed. Opt. **22**(09), 1 (2017).
14. M. Brinkmann, A. Fast, T. Hellwig, I. Pence, C. L. Evans, and C. Fallnich, "Portable all-fiber dual-output widely tunable light source for coherent Raman imaging," Biomed. Opt. Express **10**(9), 4437–4449 (2019).
15. P. Liu and Z. Zhang, "Chirped-pulse optical parametric oscillators," Opt. Lett. **43**(19), 4735–4738 (2018).
16. K. Yang, S. Zheng, P. Ye, Q. Hao, K. Huang, and H. Zeng, "Fiber-based optical parametric oscillator with flexible repetition rates by rational harmonic pumping," Opt. Express **27**(4), 4897–4906 (2019).

Optics EXPRESS

17. Y. Qin, Y. H. Ou, B. Cromey, O. Batjargal, J. K. Barton, and K. Kieu, "Watt-level all-fiber optical parametric chirped-pulse amplifier working at 1300 nm," Opt. Lett. **44**(14), 3422–3425 (2019).
18. R. K. Shelton, S. M. Foreman, L. Ma, J. L. Hall, H. C. Kapteyn, M. M. Murnane, M. Notcutt, and J. Ye, "Subfemtosecond timing jitter between two independent, actively synchronized, mode-locked lasers," Opt. Lett. **27**(5), 312–314 (2002).
19. D. J. Jones, E. O. Potma, J. Cheng, B. Burfeindt, Y. Pang, J. Ye, and X. S. Xie, "Synchronization of two passively mode-locked, picosecond lasers within 20 fs for coherent anti-Stokes Raman scattering microscopy," Rev. Sci. Instrum. **73**(8), 2843–2848 (2002).
20. K. Nose, T. Kishi, Y. Ozeki, Y. Kanematsu, H. Takata, K. Fukui, Y. Takai, and K. Itoh, "Stimulated Raman spectral microscope using synchronized Er- and Yb-fiber lasers," Jpn. J. Appl. Phys. **53**(5), 052401 (2014).
21. J. Sotor, G. Sobon, J. Tarka, I. Pasternak, A. Krajewska, W. Strupinski, and K. M. Abramski, "Passive synchronization of erbium and thulium doped fiber mode-locked lasers enhanced by common graphene saturable absorber," Opt. Express **22**(5), 5536–5543 (2014).
22. D. Popa, D. Viola, G. Soavi, B. Fu, and A. C. Ferrari, ""Graphene synchronised all-fiber laser for coherent Raman spectroscopy," in *2017 Conference on Lasers and Electro-Optics Europe & European Quantum Electronics Conference (CLEO/Europe-EQEC)*, (Germany, 2017).
23. K. Huang, J. Zeng, J. Gan, Q. Hao, M. Yan, and H. Zeng, "Passive all-optical synchronization for polarization-maintaining mode-locked fiber lasers," Opt. Express **26**(24), 32184–32193 (2018).
24. J. Zeng, B. Li, Q. Hao, M. Yan, K. Huang, and H. Zeng, "Passively synchronized dual-color mode-locked fiber lasers based on nonlinear amplifying loop mirrors," Opt. Lett. **44**(20), 5061–5064 (2019).
25. Z. Guo, Q. Hao, S. Yang, T. Liu, H. Hu, and H. Zeng, "Octave-spanning supercontinuum generation from an NALM mode-locked Yb-fiber laser system," IEEE Photonics J. **9**(1), 1–7 (2017).
26. Q. Hao, F. Chen, K. Yang, X. Zhu, Q. Zhang, and H. Zeng, "Self-started mode-locking with dispersion-imbalanced nonlinear amplifier loop," IEEE Photonics Technol. Lett. **28**(1), 87–90 (2016).
27. Y. Ozeki, W. Umemura, Y. Otsuka, S. Satoh, H. Hashimoto, K. Sumimura, N. Nishizawa, K. Fukui, and K. Itoh, "High-speed molecular spectral imaging of tissue with stimulated Raman scattering," Nat. Photonics **6**(12), 845–851 (2012).
28. J. M. Dudley, G. E. Genty, and S. E. Coen, "Supercontinuum generation in photonic crystal fiber," Rev. Mod. Phys. **78**(4), 1135–1184 (2006).
29. Y. Shen, A. A. Voronin, A. M. Zheltikov, S. P. O. Connor, V. V. Yakovlev, A. V. Sokolov, and M. O. Scully, "Picosecond supercontinuum generation in large mode area photonic crystal fibers for coherent anti-Stokes Raman scattering microspectroscopy," Sci. Rep. **8**(1), 9526 (2018).
30. Q. Li, H. Zhang, X. Shen, H. Hao, and M. Gong, "Phenomenological model for spectral broadening of incoherent light in fibers via self-phase modulation and dispersion," J. Opt. **18**(11), 115503 (2016).
31. M. Hu, C. Wang, Y. Li, L. Chai, and A. M. Zheltikov, "Tunable supercontinuum generation in a high-index-step photonic-crystal fiber with a comma-shaped core," Opt. Express **14**(5), 1942–1950 (2006).
32. Q. Jing, X. Zhang, H. Ma, Y. Huang, and X. Ren, "Improved flatness and tunable bandwidth of the supercontinuum generation in all-normal dispersion-flattened PCF using Littman-Metcalf optical bandpass filter," Opt. Laser Technol. **44**(6), 1660–1669 (2012).
33. J. Toulouse, "Optical nonlinearities in fibers: review, recent examples, and systems applications," J. Lightwave Technol. **23**(11), 3625–3641 (2005).
34. Y. Ozeki, T. Asai, J. Shou, and H. Yoshimi, "Multicolor stimulated Raman scattering microscopy with fast wavelength-tunable Yb fiber laser," IEEE J. Sel. Top. Quantum Electron. **25**(1), 1–11 (2019).
35. J. G. Porquez, R. A. Cole, J. T. Tabarangao, and A. D. Slepkov, "Brighter CARS hypermicroscopy via 'spectral surfing' of a Stokes supercontinuum," Opt. Lett. **42**(12), 2255–2258 (2017).
36. V. V. Alexander, O. P. Kulkarni, M. Kumar, C. Xia, M. N. Islam, F. L. Terry, M. J. Welsh, K. Ke, M. J. Freeman, M. Neelakandan, and A. Chan, "Modulation instability initiated high power all-fiber supercontinuum lasers and their applications," Opt. Fiber Technol. **18**(5), 349–374 (2012).
37. M. Taghizadeh, M. Hatami, H. Pakarzadeh, and M. K. Tavassoly, "Pulsed optical parametric amplification based on photonic crystal fibres," J. Mod. Opt. **64**(4), 357–365 (2017).
38. X. Hu, W. Zhang, Z. Yang, Y. Wang, W. Zhao, X. Li, H. Wang, C. Li, and D. Shen, "High average power, strictly all-fiber supercontinuum source with good beam quality," Opt. Lett. **36**(14), 2659–2661 (2011).